npj | clean water

www.nature.com/npjcleanwater

ARTICLE OPEN

Check for updates

Advanced natural hydrated iron-alum oxides cation exchange resin for simultaneous phosphate and hardness removal

Le Ba Tran[1,2,3,4], Trung Thanh Nguyen[1,2]✉, Surapol Padungthon[5], Tri Thich Le[1,2], Quynh Anh Nguyen Thi[1,2] and Nhat Huy Nguyen[2,4]✉

In this study, a hydrated iron-alum oxides-contained cation exchange resin (HIAO/225H) was synthesized for the first time from natural alum-ferric water of acid sulfate soil to improve the water quality. The HIAO/225H material was then characterized by FTIR, XRD, SEM, and EDX-mapping techniques and applied for phosphate and hardness removal tests. The phosphate removal by the HIAO/225H material reached equilibrium after 50 h with the highest adsorption capacity of 2.075 mg P g^{-1} (e.g., 69.16 mg P g^{-1} Fe) at pH 6, which was 1.12, 11.15, and 2.11 times higher than by hydrated ferric oxide/225H material, anion exchange resin (Akualite A420), and amphoteric ion exchange resin (MB6SR), respectively, under the same experimental conditions. The reason for the higher phosphate adsorption efficiency of HIAO/225H than the hydrated ferric oxide/225H material may be that HIAO contains Ca, Mg, and Al elements, leading to an easy formation of FeOOH on the surface. Particularly, HIAO/225H material was also effective for both hardness and phosphate removal with an adsorption capacity of 15.6 mg Ca g^{-1}, 9.4 mg Mg g^{-1}, and 1.825 mg P g^{-1}, which is higher 1.2 times than the phosphate removal only. This may be due to co-precipitation to form $Ca_3(PO_4)_2$ and $Mg_3(PO_4)_2$ with the support of cation exchange resins. These results showed that the HIAO/225H material has a good performance in removing both phosphate and hardness, which could be applied in practical water and advanced wastewater treatment.

npj Clean Water (2022)5:43 ; https://doi.org/10.1038/s41545-022-00188-9

INTRODUCTION

The high concentration of phosphate is one of the main causes of serious impacts on the ecological environment such as eutrophication and algal bloom which reduces the oxygen concentration in the water, harming the living environment of aquatic species[1,2]. Phosphate is released in inorganic or organic forms when entering water sources from activities such as mining, industrial agriculture, or wastewater from urban areas. Phosphate control is an essential step to maintaining ecological sustainability in the country[3,4]. According to the National technical regulation on domestic wastewater in Vietnam (QCVN 14:2008/BTNMT) with discharging water quality for water resources that are used for domestic supply purposes (Column A), the concentration of phosphate in domestic wastewater is less than or equal to 6 mg P L^{-1}. Most wastewater treatment plants have primary and secondary treatment processes that only partially remove the biodegradable organic matter through the activated sludge process. To meet the more and more strict standard requirements, modern plants have applied a tertiary treatment process with a combination of anaerobic-aerobic-anoxic processes, which increases the efficiency of phosphate removal in wastewater. However, it is difficult to control the quality of the output water due to the fluctuation in the quality of the input water, making it easy to be shocked by the sudden rise of the organic load and the need of adding a carbon source when there is a shortage. Thus, both installation and operation costs, as well as energy consumption, are high because of the large footprints of the system with many unit operations and the large amount of waste sludge generated[2,5–10]. In addition, physical and chemical processes are also applied to removing phosphate in water; however, these processes are also costly, non-selective, and more importantly, ineffective at low phosphate concentrations of less than 10 mg L^{-1}. Among the method, adsorption is usually considered a low-cost, small-footprint, and effective process for phosphate at low (or trace) concentrations[2,9,11–15]. Therefore, developing a cheap, effective, and natural nanomaterial is a very potential research interest for phosphate removal in water.

In addition, water hardness is determined mainly by the Ca^{2+} and Mg^{2+} contents, which are determined equivalently by the amount of calcium carbonate. Several studies suggest a relationship between Mg and Ca with cardiovascular disease and cancer in humans[16,17]. Therefore, several methods have been applied to remove hardness in water such as boiling, nanofiltration, reverse osmosis, ion exchange, combined ultrasonic-ion exchange, and chemical treatment with the soda-lime method[18–22]. Among them, ion exchange resins are being widely applied to the water hardness treatment process, reducing costs and bringing good treatment efficiency and adsorption is one of the most suitable methods for phosphate removal at low concentrations[23]. Recent studies on phosphate adsorption have focused on some materials such as aluminum/iron oxide-hydroxide[24], inorganic adsorbent[25,26], anion exchange resin[27,28], fly ash and activated carbon[29], and magnetic chitosan composites[30]. In addition, recent reports have shown that transition metals such as Zr(IV)[31], Fe(III)[32], and Cu(II)[2] immobilized or dispersed on resins[14,33] with strong Lewis acidity[2] and strong ligand adsorption (e.g., HPO_4^{2-} and $H_2PO_4^-$ with the oxides of polyvalent metals) exhibits phosphate adsorption selectivity with the formation of complexes via Lewis

[1]Nanomaterial Laboratory, An Giang University, 18 Ung Van Khiem St., Dong Xuyen Dist., Long Xuyen City, An Giang Province, Vietnam. [2]Vietnam National University Ho Chi Minh City, Linh Trung Ward, Thu Duc District, Ho Chi Minh City, Vietnam. [3]Faculty of Engineering - Technology - Environment, An Giang University, 18 Ung Van Khiem St., Dong Xuyen Dist., Long Xuyen City, An Giang Province, Vietnam. [4]Faculty of Environment and Natural Resources, Ho Chi Minh City University of Technology (HCMUT), 268 Ly Thuong Kiet St., Dist. 10, Ho Chi Minh City, Vietnam. [5]Department of Environmental Engineering, Khon Kaen University, 123 Moo 16 Mittraphap Rd., Nai-Muang, Muang District, Khon Kaen 40002, Thailand. ✉email: ntthanh@agu.edu.vn; nnhuy@hcmut.edu.vn

acid-base interactions[34]. The oxides of polyvalent metals such as HFeO, HZrO, and HCuO form ligands with phosphate, so these oxides can selectively adsorb phosphate from the solution containing other commonly existing anions such as Cl^-, SO_4^{2-}, and NO_3^- since these anions are only capable of complexing on the outer sphere through Coulombic interactions with the surface of metal oxides[14,33]. In recent years, the combination of mechanical strength of ion exchange resins and selectivity of iron (hydrogen)oxide for phosphate removal has been investigated to improve the strength and applicability of the materials[35,36]. The hydrated iron oxide (HFO) is harmless, readily available, inexpensive, and chemically stable over a wide range of pH conditions, which exists in the amorphous state with a size of 20–100 nm[37–39]. This HFO was reported in previous studies with high adsorption affinity for phosphate or similar oxyanions (arsenide/arsenate) in water[37,38]. In addition, our research group found that the addition of alkaline earth metal ions into the structure of iron (hydro)oxide on the cationic resin framework enhances the nitrate adsorption capacity when compared with single iron (hydo)oxide materials on cationic resin frame[40].

On the other hand, natural water from the acid sulfate soil region (called "alum-ferric water") usually contains high levels of iron, aluminum, and other compounds such as Ca, Mg, and Si due to the dissolution process when the water sources with low pH value flow through the alkaline soil[41]. The composition of alum-ferric water depends on the soil composition of the area through which the water source flows. It is commonly found in Vietnam and Southeast Asia, which usually has high concentrations of iron and aluminum and low pH values. Because alum-ferric water harms the environment, daily life, agricultural activities, and production, this water source needs to be treated to a certain level before being used for drinking, domestic, or industrial purposes[42]. Recently, our research group has proposed a way to utilize this natural alum-ferric water to synthesize iron oxide-based catalysts for heterogeneous Fenton processes[41]. In practical, the most popular and practical technique for removing aluminum, iron, and other metal cations from water is ion exchange. However, the saturated ion exchange resins contain many metals, which are usually regenerated by salts or acid. After using, the exhausted resins are usually considered hazardous waste since it contains many metals, which require intensive and costly management and treatment techniques. However, since the resin after ion exchange contains a high content of iron and other metals, it could be a very potential material source for preparing nanomaterials which is capable of removing phosphate in water.

Therefore, it is a great idea to utilize the cations from the alum-ferric water treatment for fabricating a novel hydrated iron-alum oxide/cation exchange resin material (HIAO/225H) and apply it for simultaneous removal of hardness and phosphate in water. In fact, this is a new solution to supplement the treatment (anion adsorption) capacity of cation exchange resin materials to save the space inside the pores of the ion exchange resin and reduce the volume of the resin tank. When the solution contains Ca^{2+} and Mg^{2+} ions along with phosphate ions, the material should show higher efficiency. The ion exchange adds Ca^{2+} and Mg^{2+} ions to the 225H, where these cations are partially adsorbed and precipitated on the material surface. Since both $Ca_3(PO_4)_2$ and $Mg_3(PO_4)_2$ particles can be produced during the precipitation process, the simultaneous adsorption of phosphate and hardness ions will help to increase the efficiency of the adsorption process more than the single adsorption process. In this study, HIAO/225H nanomaterial was synthesized by accumulating ions (i.e., iron and maybe others) from natural alum-ferric water of acid sulfate soil on the cation exchange resin and then applied for simultaneous removal of phosphate and hardness cations such as Ca^{2+} and Mg^{2+}. This study shows a vision in practical applicability of the material, in which cation exchange resins after treating natural alum-ferric water at individual houses could be collected and fabricated into a novel and valuable HIAO/225H adsorbent for treatment of phosphate at low concentrations and water with high hardness. Meanwhile, the process of synthesizing materials can treat the alum-ferric water so that the output water can reach surface water quality for further use. Therefore, the objective of this study is to find a suitable method for the synthesis of HIAO/225H materials from the alum-ferric water. The synthesized materials were then analyzed to explore their characteristics. The adsorption tests were then conducted to evaluate the phosphate and hardness removal of these materials in synthetic wastewater and compare with some materials of previous studies.

RESULTS AND DISCUSSION

Material synthesis and characterizations

The synthesis of HIAO/CER material was designed with a continuous flow condition with two types of strong acid cation exchange resin (Supplementary Table 1). In this study, both 225H and 220Na were used as cationic ion exchange resins. With a better phosphate adsorption capacity of 50.67 mg P g^{-1}, the 225H was chosen for the synthesis of HIAO/225H material and tested with different alum-ferric water flow rates. The results in Supplementary Tables 2 and 3 show that HIAO/225H provides a high ability for the treatment of alum-ferric water as well as the phosphate adsorption capacity of the synthesized material. Thus the 225H resin and the flow rate of 3 L h^{-1} were chosen as the suitable material and condition, respectively, for further experiments.

As seen in Fig. 1a, the characteristic peaks of Fourier-transform infrared spectroscopy (FTIR) spectrum for styrene-divinylbenzene bonds in Indion 225H cation exchange resin (225H) structure were noted. In particular, C–H bonds in benzene ring and -CH_2 in cross-linked polystyrene matrix are found at 3063 and 2923 cm^{-1}, respectively[43]. Bands of stretching vibrations at 3424 and 3385 cm^{-1} are representative of O–H bonds while the peak at 1632 cm^{-1} is characteristic of C–C bonds in the styrene ring[44]. In addition, the peak band from 843 to 1177 cm^{-1} might be assigned to the stretching vibrations of the benzene ring due to the styrene-divinylbenzene bonding matrix of the resin[45].

On the other hand, the surface chemical structure of HIAO/225H before and after adsorption was examined to clarify the adsorption mechanism occurring on the surface of the material while the FTIR spectra of fresh cation exchange resin and FeOOH (i.e., goethite and lepidocrocite) were also provided for reference purposes. As can be observed in Fig. 1a, all samples (lines 1, 2, and 3) have a peak at a wavenumber of 3390 cm^{-1}, which is assigned to the H–O–H vibration of the water of hydration. The peaks in the region of 789 and 880 cm^{-1} are characteristic of Fe–OH–Fe[46–48] while the peaks at 466 and 746 cm^{-1} are attributed to Fe–O–H[46,48]. The absorption bands at 3133 and 3384 cm^{-1} are related to the stretching vibrations of the OH groups. These results are similar to those reported in the previous studies[46,48]. In addition, the characteristic peaks in the FTIR spectrum of the phosphate-adsorbed HIAO/225H sample did not change significantly compared to the original HIAO/225H sample, except for a new peak appeared at 494.7 cm^{-1} of phosphate[49]. In addition, the FTIR spectrum of MB6SR material also shows peaks located at 1008 and 1037 cm^{-1} attributed to the $-SO_3H$ group in the resin and a strong peak at 1485 cm^{-1} of $-(CH_3)_3N^+Cl$ group, which could exchange both anions and cations in the solution (Supplementary Fig. 1 of Supplementary Data)[50,51]. Besides, the FTIR spectrum of A420 resins has a peak at 1485 cm^{-1} of $-(CH_3)_3N^+Cl$, which could only exchange with anions in the solution (Supplementary Fig. 1)[51].

As shown in Fig. 1b, there is a clear difference between the X-Ray Diffraction (XRD) patterns of the 225H and HIAO/225H, signifying the existence of HIAO particles in the 225H structure. XRD patterns of HIAO/225H materials show the nature of iron

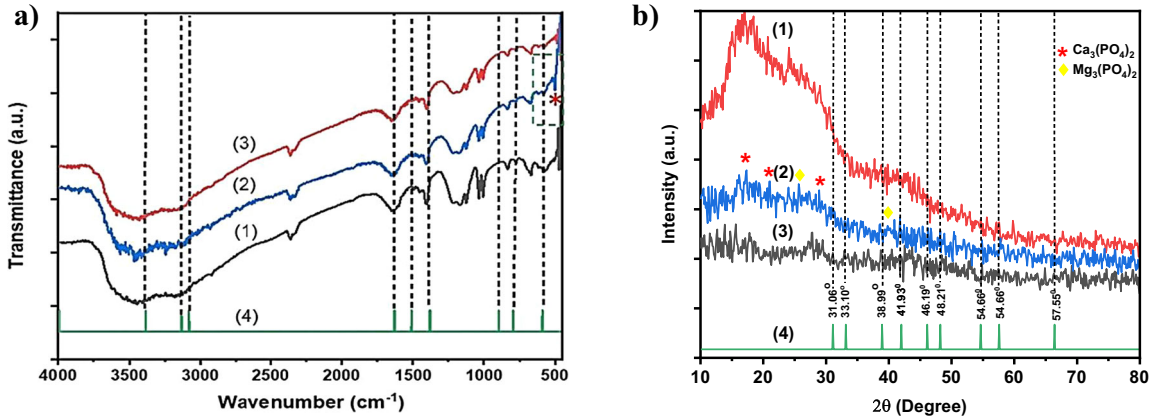

Fig. 1 FTIR spectra and XRD patterns of materials. a FTIR spectra of (1) 225H, (2) HIAO/225H after phosphate adsorption, (3) fresh HIAO/225H, (4) lepidocrocite and goethite references[48,49]. **b** XRD patterns of (1) 225H, (2) HIAO/225H after phosphate adsorption, (3) fresh HIAO/225H, and (4) iron oxide-hydroxide reference (JCPDS card no. 18-0639)[54]).

Table 1. Elemental composition (wt%) of material as determined by EDX.

Material/elements	Resin (wt%)	Fresh HIAO/225H (wt%)	HIAO/225H after adsorption (wt%)
C	45.22 ± 0.08	31.62 ± 0.06	31.37 ± 0.05
O	54.78 ± 0.19	34.63 ± 0.11	34.97 ± 0.09
Fe		33.14 ± 0.27	32.18 ± 0.22
Al		0.30 ± 0.01	0.36 ± 0.01
Ca		0.11 ± 0.01	0.12 ± 0.01
Mg		0.20 ± 0.01	0.25 ± 0.01
P			0.75 ± 0.02

hydrated oxide nanomaterial (FeOOH). The observed characteristic peaks at 2θ of 31.06, 33.10, 38.99, 41.93, 46.19, 48.21, 54.66, and 57.55° indicate the orthorhombic iron oxide-hydroxide structure of the HIAO/225H material (JCPDS card no. 18-0639, Fig. 1b)[52]. However, the peaks are of low intensity and therefore suffer interference from the background noise, implying that HIAO materials synthesized by this method have a low crystallinity. This is possibly due to the low-temperature synthesis of this material without any calcination for the crystallization of iron oxide-hydroxide, which is commonly observed for ferric (hydrogen)oxide materials on ion-exchange resin substrates[9]. Other materials such as Fe/225H, Fe-Mg/225H, and Fe-Ca/225H also give similar results as HIAO/225H material (Supplementary Fig. 2). In addition, the XRD spectrum of the HIAO/225H sample after phosphate adsorption is similar to that of the fresh HIAO/225H sample, demonstrating that phosphate adsorption does not change the structure of the material of the HIAO/225H sample, which is very similar to those observed in the FTIR results. In addition, the existence of $Ca_3(PO_4)_2$ and $Mg_3(PO_4)_2$ in HIAO/225H after phosphate adsorption was determined according to JCPDS Card No. 861585 and 01-0941 as shown in Line 2 of Fig. 1b.

The morphology and surface elemental composition of the materials were examined by scanning electron microscope (SEM) and energy-dispersive X-ray spectroscopy mapping (EDX-mapping), respectively. The 225H has a spherical morphology (Supplementary Fig. 3) with a basic chemical composition of organic structure (Supplementary Table 6 and Table 1). For the HIAO/225H material, the composition of the elements on the surface of the materials is summarized in Table 2 with the main components of C, O, Fe, Ca, Mg, and Al. Phosphate was only detected in the structure of the HIAO/225H material after

Table 2. The kinetic models for phosphate adsorption using HIAO/225H.

Model	Parameter	Parameters
Pseudo-first-order	K_{ad} (g mg^{-1} h^{-1})	0.0756
	R^2	0.9802
	Q_e, cal:	
	(mg P g^{-1} Fe)	66.47
	(mg P g^{-1})	1.9941
	Q_e, exp:	
	(mg P g^{-1} Fe)	69.15
	(mg P g^{-1})	2.075
Pseudo-second-order	K_{ad} (g mg^{-1} h^{-1})	0.001494
	R^2	0.9906
	Q_e, cal:	
	(mg P g^{-1} Fe)	79.37
	(mg P g^{-1})	2.3811
Intraparticle diffusion	K (g mg^{-1} h$^{-0.5}$)	0.2618
	C	0.2939
	D (cm^2 s^{-1})	7.4405×10^{-10}
	R^2	0.9527
Film diffusion	D (cm^2 s^{-1})	2.9439×10^{-5}
	R^2	0.9724
Pore diffusion	D (cm^2 s^{-1})	8.7516×10^{-6}
	R^2	0.8176

phosphate adsorption (Supplementary Fig. 4), but not in those of the resin (Supplementary Fig. 3) and fresh HIAO/225H material (Supplementary Fig. 5). In general, the shape of all materials is spherical, which is similar to the shape of the original 225H material. Interestingly, HIAO/225H materials have a higher Fe composition than Ca, Mg, and Al elements, and the composition of this material is very similar to the composition of elements in alum-ferric water, which is the raw material for synthesizing HIAO/225H material. In addition, the SEM-mapping results (Supplementary Fig. 5) show that the HIAO particles are located inside the pores and evenly coated on the surface of the 225H resin. Besides, the (hydrogen) oxide components of Fe, Al, Ca, and Mg are also evenly distributed on the surface of the resin. However, the composition of elements such as Al, Ca, and Mg is difficult to be determined by the XRD

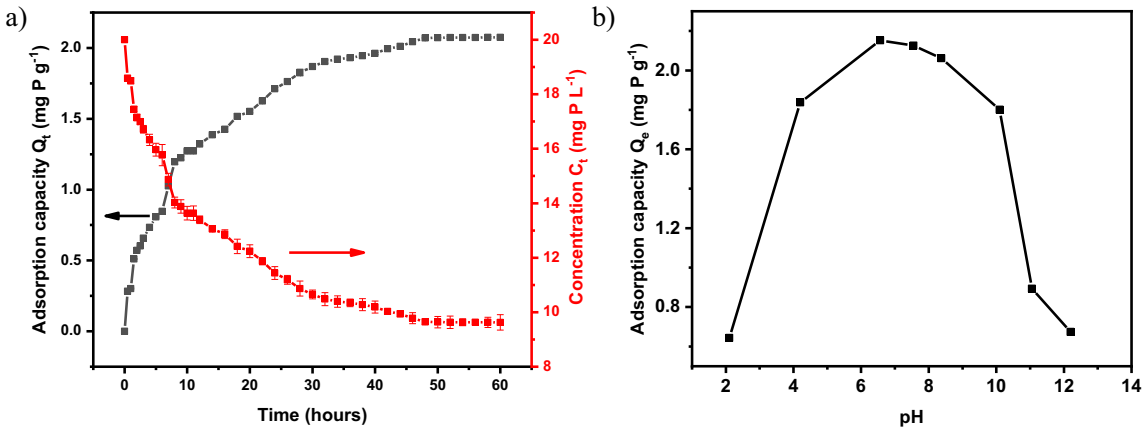

Fig. 2 Effect of time and pH on the adsorption of phosphate. a Effect of time on the adsorption of phosphate with condition: 5 g (HIAO/225H)/L, 20 mg P L^{-1}, pH 6.0, room temperature of ~30 °C). **b** Effect of pH on the adsorption of phosphate with condition: 50 h, 5 g (HIAO/225H)/L, 20 mg P L^{-1}, and room temperature of ~30 °C; and experimental condition ($n = 3$ ±standard deviation [s.d.]).

technique, which may be due to the relatively low contents of these elements as compared to other elements.

The results obtained in the physicochemical analysis of HIAO/225H materials reveal that the simple but effective method proposed in this study can be applied to the synthesis of natural HIAO/225H materials. A generalization for the synthesis of materials can be suggested by the following reaction equations (Reactions 1–9):

Step 1. Adsorption of metal ions onto 225H surface via ion exchange

$$\overline{3R(SO_3^-)H^+} + Fe^{3+} \rightarrow \overline{[R(SO_3^-)]_3Fe^{3+}} + 3H^+ \quad (1)$$

Other reactions also simultaneously occur on the surface of the material:

$$\overline{3R(SO_3^-)H^+} + Al^{3+} \rightarrow \overline{[R(SO_3^-)]_3Al^{3+}} + 3H^+ \quad (2)$$

$$\overline{2R(SO_3^-)H^+} + Ca^{2+} \rightarrow \overline{[R(SO_3^-)]_2Ca^{2+}} + 2H^+ \quad (3)$$

$$\overline{2R(SO_3^-)H^+} + Mg^{2+} \rightarrow \overline{[R(SO_3^-)]_2Mg^{2+}} + 2H^+ \quad (4)$$

Step 2. Generation of iron-alum hydroxide

$$\overline{[R(SO_3^-)]_3Fe^{3+}} + 3NH_4OH \rightarrow \overline{3R(SO_3^-)NH_4^+ - Fe(OH)_3} \quad (5)$$

Other reactions also occur at the same time:

$$\overline{[R(SO_3^-)]_3Al^{3+}} + 3NH_4OH \rightarrow \overline{3R(SO_3^-)NH_4^+ - Al(OH)_3} \quad (6)$$

$$\overline{[R(SO_3^-)]_2Ca^{2+}} + 2NH_4OH \rightarrow \overline{2R(SO_3^-)NH_4^+ - Ca(OH)_2} \quad (7)$$

$$\overline{[R(SO_3^-)]_2Mg^{2+}} + 2NH_4OH \rightarrow \overline{2R(SO_3^-)NH_4^+ - Mg(OH)_2} \quad (8)$$

And at this stage, iron-alum hydroxide is defined as a mixture of metal hydroxides. Thus, iron-alum hydroxide has the molecular formula $Fe_xM_y(OH)_z$ (where M = Al, Ca, Mg, …). In summary, the general formula of iron-alum hydroxide particles located in the pores of 225H is represented as: $\overline{nR(SO_3^-)NH_4^+ - Fe_xM_y(OH)_z}$

Step 3. Formation of hydrated iron-alum oxide

$$\overline{nR(SO_3^-)NH_4^+ - Fe_xM_y(OH)_z} \rightarrow \overline{nR(SO_3^-)NH_4^+ - Fe_xM_y(OOH)_z} \quad (9)$$

Noticeably, the quality of iron-alum contaminated water from the natural acid sulfate soil after passing through the cationic exchange resin column reached the surface water standard of QCVN 08-MT:2015/BTNMT—Column A (Supplementary Table 3). This is a very meaningful method to improve the quality of natural surface water under the impact of natural pollution (e.g., alum-ferric contamination). In addition, the 225H material can be used with multifunction as (1) a filter material to remove ions in contaminated water and (2) a substrate that provides pores (e.g., in the resin matrix) for the formation of HIAO particles (Supplementary Fig. 5). The phosphate adsorption experiment was then designed to better understand the performance of HIAO material while the simultaneous adsorption of phosphate and removal of hardness was for evaluating the practical applicability of this material.

Adsorption of phosphate onto HIAO/225H

Figure 2a shows that the adsorption capacity of HIAO/225H increased with increasing adsorption time during 60 h of investigation. Basically, there are 3 basic stages in phosphate adsorption using HIAO/225H material, including the first stage of the fast adsorption process in the first 10 h, the second stage of slow adsorption in the next 40 h, and the last stage of equilibrium after 50 h of adsorption with an adsorption capacity of 2.075 mg P g^{-1}. Therefore, it shows that the HIAO/225H material has the same adsorption time as the previous studies[53]. This may indicate that the adsorption process based on FeOOH material plays a major role as compared to other oxides presented in the structure of HIAO material, which is also compatible with the results of composition analysis of HIAO/225H materials. The kinetics for the adsorption of phosphate onto HIAO/225H were then studied by using three kinetic models of pseudo-first-order, pseudo-second-order, and intraparticle diffusion models[53–56], as presented in Table 2. Based on the correlation coefficient ($R^2 > 0.9$), all three models can be used for describing the adsorption of phosphate. However, the pseudo-second-order model is the most suitable adsorption model for phosphate adsorption using HIAO/225H since it has the highest R^2 value of 0.9906 (Supplementary Fig. 6) with similar values of calculated and experimented adsorption capacity. Besides, the K adsorption rate constant was also determined to be 0.001494 (g mg^{-1} h^{-1}) at a phosphate concentration of 20 mg L^{-1}.

As also observed in Fig. 2a, after 10 h of rapid adsorption, the adsorption capacity increased slowly to 50 h. After 50 h, the adsorption capacity did not change much during the treatment process. Meanwhile, the concentration of the adsorbent decreases with time, and after 50 h, the concentration has almost no change. The most reasonable time for the phosphate adsorption is 50 h, which was then chosen for all further experiments in this study. The diffusion models are also provided in Table 2, including intraparticle diffusion, film diffusion, and pore diffusion. Among them, the

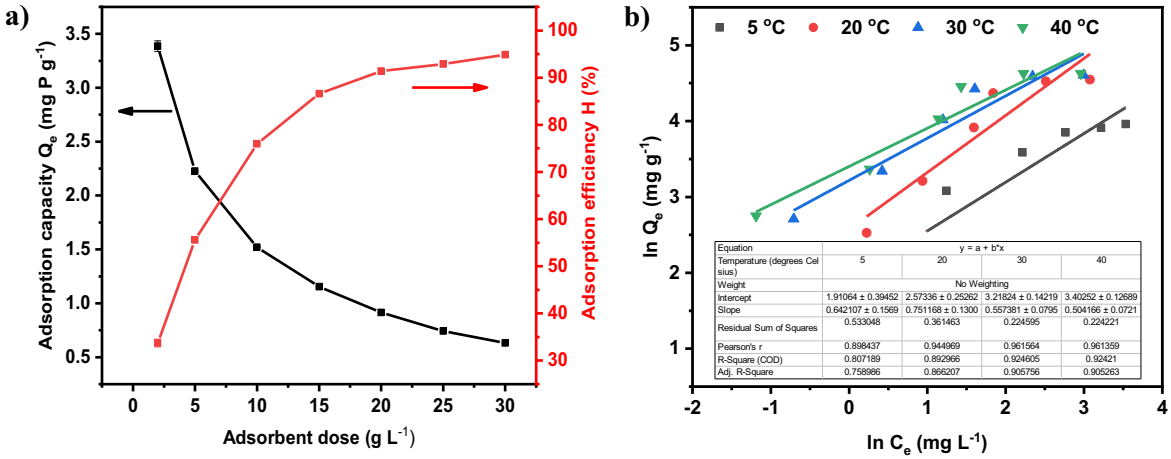

Fig. 3 Effect of dosage and the isotherm plot of Freundlich for the adsorption of phosphate. a Effect of dosage on the adsorption of phosphate with experimental conditions: 50 h, 20 mg P L^{-1}, pH 6.0, and room temperature of ~30 °C; **b** the isotherm plot of Freundlich for the adsorption of phosphate with experimental conditions: 50 h, 10 g (HIAO/225H)/L, pH 6.0 room temperature of ~30 °C; and experimental condition ($n = 3$ ±standard deviation [s.d.]).

intraparticle diffusion model shows a diffusion coefficient of 7.4405×10^{-10} (cm^2 s), which is much lower than those in the other models. This suggests that intraparticle diffusion is a controlling step in the adsorption of phosphate and the adsorption of phosphate has several stages as illustrated in Fig. 2a.

Previous studies have shown that solution pH is an important parameter that affects the adsorption capacity of the materials[9,34,56]. In this study, the phosphate adsorption capacity of the materials from pH 2 to 12 is shown in Fig. 2b. The adsorption capacity increased gradually from pH 2 to 6, where it reached the highest value of 2.067 mg P g^{-1}. In addition, the point of zero charge (pH_{pzc}) of the material was determined at 6 (Supplementary Fig. 7). When the pH is <6.5, the surface of the material has a positive charge that favors the adsorption of phosphates, which are negatively charged in the forms of HPO_4^{2-} and $H_2PO_4^-$ (Reactions 10–12) and retained by iron oxyhydroxide through the formation of a complex inside the pores of 225H. Since HPO_4^{2-} tends to form stronger amphoteric complexes than $H_2PO_4^-$ (Reactions 15, 16), lowering the pH causes more phosphate to remain in the form of $H_2PO_4^-$ with a less negative charge, resulting in an unfavorable condition for the adsorption process. Besides, too low pH values decrease the negative charge of phosphate from divalent to monovalent, thus reducing the electrostatic attraction between the positively charged iron oxyhydroxide groups and the phosphate ions. The adsorption capacity then decreased gradually when the pH exceeded 6 and reached only 22.45 mg P g^{-1} Fe at pH 12. At these high pH conditions, HIAO is deionized and negatively charged (Reactions 13, 14); therefore, the electrostatic repulsion and Donnan co-ion exclusion inhibit phosphate adsorption[8,9].

$$H_3PO_4 \leftrightarrows H^+ + H_2PO_4^- \qquad pKa_1 = 2.15 \tag{10}$$

$$H_2PO_4^- \leftrightarrows H^+ + HPO_4^{2-} \qquad pKa_2 = 7.20 \tag{11}$$

$$HPO_4^{2-} \leftrightarrows H^+ + PO_4^{3-} \qquad pKa_3 = 12.35 \tag{12}$$

$$Fe\overline{O}H_2^+ \leftrightarrows Fe\overline{O}H + H^+ \qquad pKa_1 = 6.5 \tag{13}$$

$$Fe\overline{O}H \leftrightarrows FeO^- + H^+ \qquad pKa_2 = 8.5 \tag{14}$$

$$Fe\overline{O}H_2^+(Cl^-) + H_2PO_4^- \leftrightarrows Fe\overline{O}H_2^+ : H_2PO_4^- + Cl^- \tag{15}$$

$$Fe\overline{O}H_2^+(Cl^-) + HPO_4^{2-} \leftrightarrows 2(Fe\overline{O}H_2^+) : HPO_4^{2-} + 2Cl^- \tag{16}$$

As illustrated in Fig. 3a, the adsorption capacity of phosphate is affected by the dose of HIAO/225H adsorbent. As the adsorbent dose increased, the adsorption capacity decreases while the adsorption efficiency increased gradually and the output water quality was improved. For example, the phosphate adsorption capacity decreased rapidly when the adsorbent dosage increased in the range of 2 to 10 g L^{-1} and then decreased slowly in the adsorbent dosage range of 10–30 g L^{-1}. This can be explained that the number of ions in the solution being constant, but the adsorption capacity is the amount of ions per amount of adsorbent material, so when increasing the amount of adsorbent, the capacity decreases. To meet the standard of QCVN 14:2008/BTNMT (Column A) with an output phosphate concentration of lower than 6 mg P L^{-1}, the appropriate adsorbent dosage should be selected as 10 g L^{-1} for the next experiments.

Figure 3b demonstrates the influence of phosphate concentration and temperature on the adsorption capacity of the HIAO/225H material. As the concentration increases, the adsorption capacity also increases gradually. This is because increasing the concentration will lead to an increase in the concentration gradient between the contact solution and the pores of the ion exchange resin, leading to an increase in the adsorption of ions on the adsorbent. Similarly, the increase in temperature causes an increase in the mobility of phosphate ions, thus favoring phosphate adsorption. This can be seen clearly in solutions with an initial concentration from 5 to 50 mg P L^{-1} at different temperatures of 5, 20, 30, and 40 °C, which is similar to previously published studies[15,57].

In addition, in the study of adsorption process characteristics, it has been shown that determining the adsorption isotherms is an important step. Usually, Langmuir and Freundlich isotherm models were used to describe the relationship between the phosphate on the surface of the material and its equilibrium concentration in the solution at a constant temperature[58,59]. The adsorption isotherm parameters of the processes are presented in Supplementary Table 7. Although both Langmuir and Freundlich models are suitable to describe phosphate adsorption at 30 and 40 °C, the Langmuir model is more suitable because of its higher correlation coefficient with R^2 of 0.9788. In addition, the K_L value, which is the Langmuir constant representing the affinity of the adsorbent and the surface of the adsorbent[55,56,60], was calculated from the equations (i.e., $y = 0.0082x + 0.0296$ and $y = 0.0084x + 0.0223$) to be 0.277 and 0.377 L mg^{-1} at 30 and 40 °C, respectively. The comparison of the suitability of the two adsorption models is seen more clearly through the χ^2 value. The χ^2 values of the Langmuir model for phosphate (5.009–12.452) are much lower than those of the Freundlich model for phosphate (11.309–26.686). The χ^2 value of

the Langmuir model at 30 °C is the lowest one (5.009) since its modeled data are similar to the experimental data.

On the other hand, the thermodynamic property of the adsorption process is expressed through parameters such as Gibbs free energy (ΔG), entropy (ΔS), and enthalpy (ΔH) using equilibrium constants at different temperatures (e.g., 5, 20, 30, and 40 °C) are summarized in Supplementary Table 4. ΔG is a value that can indicate whether a material is physically or chemically adsorbed. The ΔG values from −20 to 0 kJ mol^{-1} suggest a physical adsorption process and those from −80 to −400 kJ mol^{-1} suggest chemisorption[61]. The ΔG in this study was estimated to be −3.416, −5.372, −6.677, and −7.981 kJ mol^{-1} at 5, 20, 30, and 40 °C, respectively, indicating that the adsorption process was spontaneous at all experimented temperatures[56], which can be classified as a physical adsorption process. Regarding the interaction between phosphate ions and HIAO/225H surface during the adsorption process, van der Waals forces, hydrogen bonds, ionic pairs, and other polar and nonpolar interactions should play an important role[56,61,62]. The ΔH value calculated from the equation is 32.849 kJ mol^{-1}, and this positive value shows that this is an endothermic adsorption process. The value of ΔS is greater than 0, implying that there are increases in affinity and contact between the adsorbate and adsorbent in the adsorption process[62].

Effect of coexisting ions, durability, and real wastewaters

In water and wastewater, the Cl^-, SO_4^{2-}, NO_3^-, and HCO_3^- anions are usually co-existed with PO_4^{3-} anion. Thus, it is necessary to study the influence of these ions on the efficiency of the phosphate adsorption process. Figure 4 shows the effect of anions on the adsorption capacity of phosphate using HIAO/225H material. Among the anions, HCO_3^- (with a concentration of 100 mg L^{-1}) had the most influence on the phosphate adsorption capacity of the material. Meanwhile, other anions such as Cl^-, NO_3^-, and SO_4^{2-} had no obvious effect on the adsorption process, proving the selective interaction and adsorption of the HIAO/225H material with HCO_3^- and PO_4^{3-} anions[14,33]. In general, the HIAO/225H material has low selectivity and this is a common feature of materials with physical adsorption characteristics. On the other hand, the presence of HCO_3^- ion showed great competition for the phosphate adsorption process of the material. This may be because the HCO_3^- ion present in the solution could be adsorbed on the surface of the HIAO/225H material, which can form unexpected products such as $MgCO_3$ and $CaCO_3$. Therefore, this changed the environment inside the resin pores which affects the presence of FeOOH, which can be further seen via the

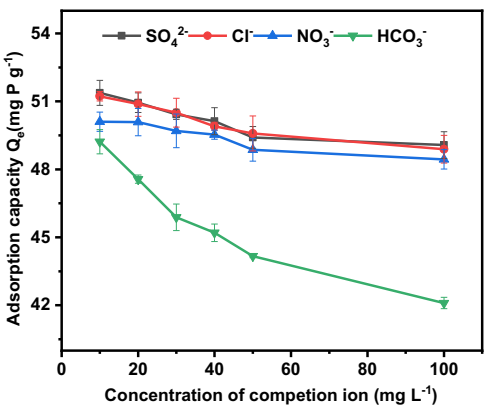

Fig. 4 Effect of other anions on the adsorption of phosphate. Experimental conditions: 50 h, 10 g (HIAO/225H)/L, 20 mg P/L, pH 6.0, room temperature of ~30 °C; and experimental condition ($n = 3$ ±standard deviation [s.d.]).

enhancement mechanism of phosphate adsorption efficiency in the later section. Thus, when researching and applying this material to water and wastewater treatment, it is necessary to pay attention to the selectivity of anion adsorption in the aqueous environment.

Regarding cations in solution, the presence of calcium and magnesium in the solution increases the phosphate adsorption, as evidenced in Supplementary Fig. 8. At the same time, the material was also capable of removing Ca from 224 to 68 mg L^{-1} and Mg from 185 to 91 mg L^{-1}. The phosphate adsorption capacity was enhanced 1.2 times under the presence of Ca and Mg, up to 1.825 mg P g^{-1} resin. This can be explained by the integration of Ca and Mg onto the surface of CER by ion exchange (Reactions 3, 4), as illustrated in Fig. 5A, which then adsorb phosphate to form $Ca_3(PO_4)_2$ and $Mg_3(PO_4)_2$ (Reactions 17, 18), as evidenced by XRD and FTIR (Fig. 1a, b). $Ca_3(PO_4)_2$ and $Mg_3(PO_4)_2$ detach from the surface of resin and accumulate on the surface of HIAO (Fig. 5B). In comparison, the solution consisting of phosphate, Ca^{2+}, and Mg^{2+} maintained at atmospheric conditions for 50 h (Supplementary Fig. 9) without adding material shows that the content of these ions was still stable without any homogenous reactions, proving that the changes in the contents of phosphate, Ca^{2+}, and Mg^{2+} ions when adding materials are all due to adsorption or ion exchange. Thus, it can be said that the presence of Ca^{2+} and Mg^{2+} ions in the solution can increase the phosphate removal efficiency of HIAO/225H materials thanks to the precipitation of $Ca_3(PO_4)_2$ and $Mg_3(PO_4)_2$ on the solid surface or with the support of the solid surface. This is similar to the process of crystallization of precipitates on the surface of the nuclei in the synthesis of nanomaterials by wet chemistry. In addition, in the presence of Ca and Mg in solution, the HIAO/225H material showed a total capacity of 26.825 mg g^{-1} resin as compared to 12.7 mg g^{-1} when using MB6SR amphoteric ion exchange material. Furthermore, the removal ability of Ca^{2+} and Mg^{2+} in the solution of HIAO/225H material (25 mg g^{-1}) is also about 5 times higher than that of MB6SR material (5.1 mg g^{-1}) (Supplementary Table 8).

$$\overline{\left[R(SO_3^-)\right]_2Ca^{2+}} + PO_4^{3-} \rightarrow \overline{2R(SO_3^-)Me - Ca_3(PO_4)_2} \quad (17)$$

$$\overline{\left[R(SO_3^-)\right]_2Mg^{2+}} + PO_4^{3-} \rightarrow \overline{2R(SO_3^-)Me - Mg_3(PO_4)_2} \quad (18)$$

The adsorption capacity of HIAO/225H materials was compared with similar and/or commercial materials such as Ca-Fe/225H, Mg-Fe/225H, Al-Fe/225H, Fe/225H (i.e., HFO/225H), 225H, and Akualite A420 (Supplementary Fig. 10). The 225H material is completely incapable of phosphate adsorption while HIAO/225H materials gave 1.126 times higher adsorption capacity than HFO/225H. To better understand this process of improving adsorption efficiency, the evaluation of Ca-Fe/225H, Mg-Fe/225H, and Al-Fe/225H composites was carried out to investigate the phosphate adsorption process. The order of phosphate adsorption capacity of the materials is Ca-Fe/225H > Mg-Fe/225H > HIAO/225H > Al-Fe/225H > HFO/225H. It can be concluded that the existence of alkaline earth metal ions and amphoteric metal ions in the HFO structure enhances the phosphate adsorption capacity of the material. In addition, the FTIR spectrum in Supplementary Fig. 11 shows that the intensity of the peak at wavenumber 3184 cm^{-1} (characteristic for vibrations of the -OH group) is corresponding to the above order of adsorption capacity. Therefore, it can be said that the presence of alkaline and amphoteric ions increase the possibility of Fe–OOH formation, thus their presence is likely to increase the phosphate adsorption efficiency of the HFO. In this case, thanks to the existence of Ca, Mg, and Al elements in the structure of HFO, HIAO/225H material shows superior phosphate adsorption capacity as compared to HFO/225H materials, as demonstrated in Fig. 6.

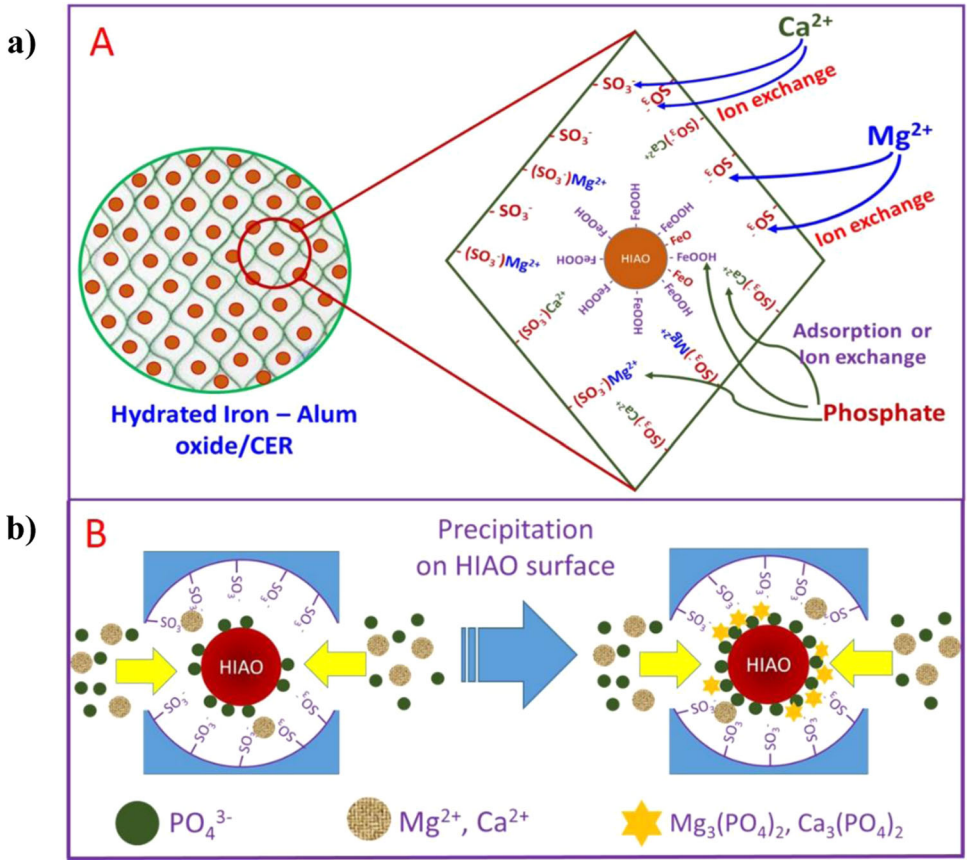

Fig. 5 Illustrations of simultaneous adsorption and precipitation of HIAO/225H material. a Simultaneous adsorption of phosphate and hardness; **b** precipitation of $Ca_3(PO_4)_2$ và $Mg_3(PO_4)_2$ on HIAO surface of HIAO/225H material.

It is demonstrated that HIAO/225H materials can simultaneously adsorb anions and cations. This is a novel method to add a new capability (e.g., anion adsorption) of 225H material and saves the empty volume inside the pores of the resin and the total volume of required ion exchange resin. In the simultaneous presence of Ca^{2+}, Mg^{2+}, and phosphate ions, HIAO/225H showed higher adsorption capacity than in the solution of phosphate only or higher than the primitive 225H. This can be explained previously, which is more detailedly demonstrated via a mechanism in Figs. 5, 6, as follows. The neighboring Ca^{2+} and Mg^{2+} ions are attached to the 225H resin through ion exchange and also adsorbed and partially precipitated on the surface of HIAO particles to form $Ca_3(PO_4)_2$ and $Mg_3(PO_4)_3$ particles. Therefore, the simultaneous adsorption of phosphate and hardness ions helps to increase the efficiency of the adsorption process as compared to the single phosphate adsorption process.

The HIAO/225H material was then applied to domestic wastewater treatment. As exhibited in Supplementary Fig. 12, the phosphate concentration reduced from 20 to 4.76 mg P L^{-1} for synthetic wastewater and from 12.4 to 1.53 mg P L^{-1} for domestic wastewater, both met the standards of QCVN 14: 2008/BTNMT (Column A). Although there may be competing ions in domestic wastewater, the competition does not greatly affect the phosphate adsorption process, showing the high selectivity of the material for phosphate adsorption.

The durability, stability, and reusability of the material were evaluated via cycle tests (Supplementary Fig. 13) and the regeneration mechanism is proposed in Fig. 7. When using only NH_4OH solution for regeneration (Supplementary Fig. 13), the adsorption capacity after five times reuse was only 0.5 mg P g^{-1}, equivalent to 25–30% capacity as compared to the fresh material. Thus, the regeneration ability of NH_4OH is not acceptable and needs further study to find out a more effective regeneration way. Results from FTIR and XRD analysis (Fig. 1a, b) showed that the phosphate-saturated adsorbent materials are determined to have the presence of products such as $Ca_3(PO_4)_2$ and $Mg_3(PO_4)_2$. Therefore, it is difficult to recover the materials with NH_4OH only. Hence, a new regeneration method was tested, which has two steps: (i) cleaning the surface of HIAO material with HCl solution (3 vol.%) and (ii) reverting the functional group on the HIAO surface with NH_4OH solution (Fig. 7). With HCl and NH_4OH regeneration, the adsorption capacity after 10 cycles is about 80% compared to the initial adsorption (Supplementary Fig. 13). Therefore, HCl washing step significantly improves the regeneration of HIAO/225H materials although more intensive work is needed to obtain an optimal method for the regeneration of HIAO/225H after simultaneous removal of phosphate and hardness.

Comparison with other studies

The phosphate adsorption capacity of the materials in the study was also compared with the results of previous publications, as can be seen in Supplementary Table 5. Although the phosphate adsorption capacity of HIAO/225H was not high, it is still very potential as a cheap material since it is a waste from water treatment. The most possible use of the HIAO/225H could be in rural areas, where it can be used for simultaneously removing phosphate and hardness in water.

Environmental implication

This study successfully synthesized HIAO/225H material capable of removing phosphate and hardness in water. This material was synthesized from natural polluted alum-ferric water of acid sulfate

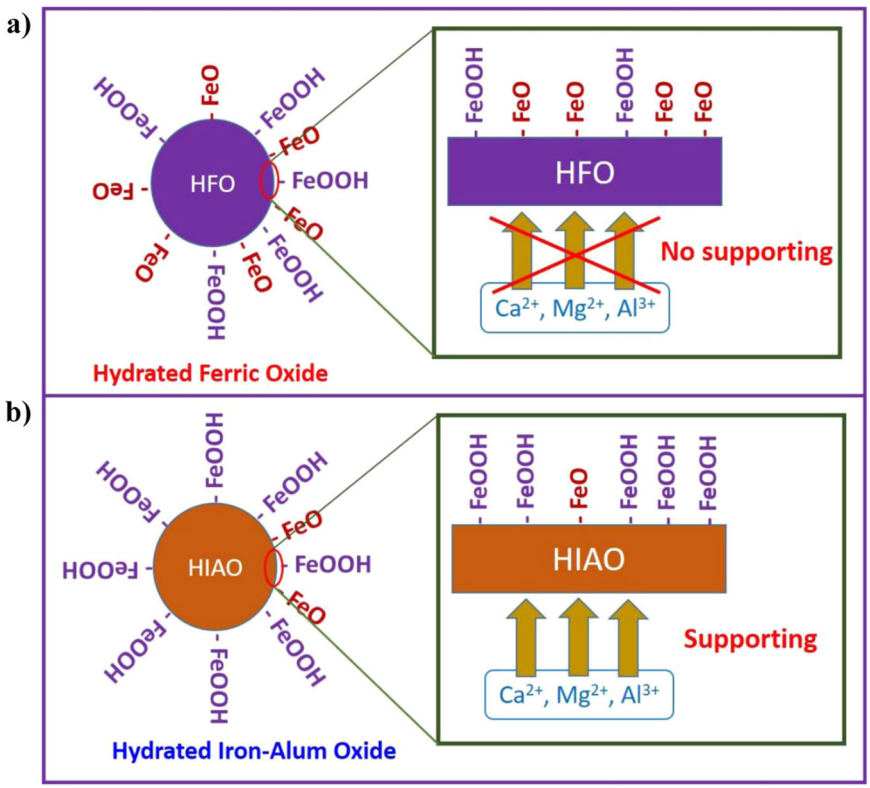

Fig. 6 Mechanism for the enhanced formation of FeOOH on the surface of HIAO. a The surface of the material without the presence of ions: Ca^{2+}, Mg^{2+}, and Al^{3+}. **b** The surface of the material has the presence of ions: Ca^{2+}, Mg^{2+}, and Al^{3+}.

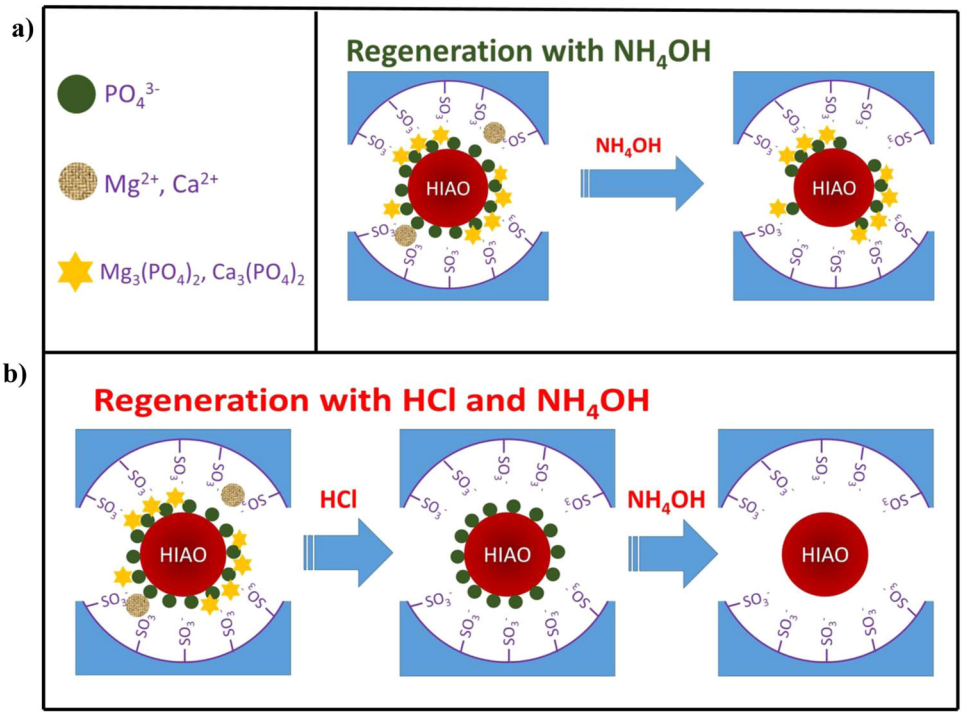

Fig. 7 Mechanism for the regeneration of HIAO/225H material. a The material after the adsorption process was regenerated with NH_4OH solution. **b** The material after the adsorption process was regenerated with HCl and NH_4OH solution.

soil. This provides a simple ion exchange method for treatment of naturally contaminated alum-ferric water from acid sulfate soil. After that, the saturated ion exchange material was effectively applied for the treatment of phosphate and hardness in wastewater.

Conclusions and discussion

The HIAO/225H material was successfully synthesized from natural alum-ferric and applied for phosphate and hardness removal in water. The equilibrium adsorption time was determined to be 50 h

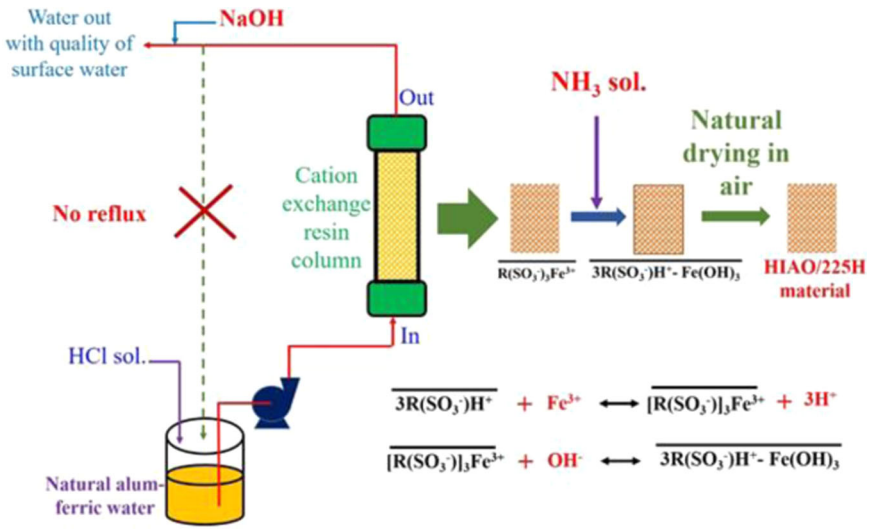

Fig. 8 Process of HIAO/225H material synthesis. A plastic column with a diameter of 1 cm, cation exchange resin: 5 g, adding HCl into the natural alum-ferric water with a dose of 1 mL L^{-1}, a flow rate of 3 L h^{-1}, ammonia solution: 100 mL of deionized water containing 1 mL of ammonia solution (28–34 vol%), NaOH solution (0.1 M).

while the suitable pH was around 6. The HIAO/225H showed the adsorption capacity increased with the increase of phosphate concentration and adsorption temperature. In addition, HIAO/225H material showed that the phosphate adsorption efficiency was 1.126 times higher than that of material HFO/225H. This would be due to the existence of Ca, Mg, and Al elements in the structure of HIAO material, which facilitates the formation of FeOOH and thus the efficiency of phosphate adsorption is improved. On the other hand, in the simultaneous phosphate and hardness adsorption by HIAO/225H material, the presence of Ca and Mg cations in the solution enhanced the phosphate adsorption up to 1.2 times compared with a solution without phosphate, possibly due to the support of the solid surface for enhanced precipitation. Therefore, this is a potential material with a large source of natural materials (alum-ferric water). In both synthetic and domestic wastewater, the HIAO/225H was effective for removing phosphate to meet the discharging standards, indicating the practicability of the material in wastewater treatment. This research is not only to synthesize materials to treat phosphate and hardness but also to treat alum-ferric water in nature.

METHODS

Chemicals

Chemicals used in the study such as NH_4Cl, NH_3 solution (28–34 vol%), and NaCl were from China, and HCl, KH_2PO_4, KCl, K_2SO_4, $MgCl_2$, KNO_3, and $CaCl_2$ were from Merck. Supplementary Table 6 of Supplementary Data shows the properties of ion exchange resin used in this work, including cation exchange resin H^+ (225H) and Na^+ (220Na) from India, anion change resin of Akualite (A420) from China, and cation-anion resin of Indion (MB6SR) from India. Deionized water was taken from a local machine in the laboratory. The phosphate solution was prepared by dissolving KH_2PO_4 into deionized water.

Material synthesis and characterizations

The HIAO/225H materials were synthesized based on the principle of ion exchange between ions in cation exchange resin (225H) and ions in alum-ferric water using a continuous flow reactor. Interestingly, the quality of alum-ferric water after flowing through the ion exchange resin column meets the National technical regulation on surface water quality (QCVN 08-MT:2015/BTNMT) for domestic water supply purposes in Column A (Supplementary Table 3).

As depicted in Fig. 8, 5 g of 225H cation exchange resin was first placed in a plastic column with a diameter of 1 cm. The water sample was then prepared by adding HCl into the natural alum-ferric water with a dose of 1 mL L^{-1}. This natural alum-ferric water was subsequently passed through the cation exchange column from bottom to top with a flow rate of 3 L h^{-1} until the column turned red and the color of outlet water was similar to the inlet (brown-red color). After that, the ion exchange resin was removed from the column and washed several times to remove the external residues. The resin was then added to 100 mL of deionized water containing 1 mL of ammonia solution (28–34 vol%) and stirred at 500 rpm for 10 min. Next, the resin was separated from the solution and washed several times with deionized water. Finally, the material was naturally dried in the air, where it turned to a yellow-orange or red color.

The morphology of the material was observed by scanning electron microscopy (SEM, JCM-7000, JEOL, Japan). The elemental compositions were determined by energy-dispersive X-ray analysis (EDX) and EDX-mapping. The surface chemistry was characterized by Fourier-transform infrared spectroscopy (FTIR, Alpha, Bruker, Germany). The crystal phase and crystalline structure of the materials were examined by X-ray diffraction (XRD, AERIS, Malvern Panalytical, Netherlands).

Adsorption tests

The application of the material was evaluated via its adsorption ability for phosphate and other cations (i.e., Mg and Ca) using batch adsorption experiments. For the single phosphate adsorption test, 0.25 g of material was added to 50 mL of phosphate solution (20 mg P L^{-1}) and let adsorption for 60 h. The material was then removed and the solution was sent for analyzing phosphate concentration by using UV-Visible spectroscopy (V-730 UV, JASCO, Japan). The investigated parameters include contact time (0–60 h), adsorbent dosage (2–30 g L^{-1}), solution pH (2–12), and competing ions in solution (i.e., sulfate, bicarbonate, chloride, and nitrate), initial phosphate concentration (5–50 mg L^{-1}), and temperature (5–40 °C). The phosphate adsorption efficiency (H, %)

and adsorption capacity (Q_e, mg P g^{-1}) are calculated by the following equations.

$$H = \left(1 - \frac{C_t}{C_o}\right) \times 100\% \quad (19)$$

$$Q_e = \frac{(C_o - C_e) \times m}{V} \quad (20)$$

Where C_o, C_t, and C_e are phosphate concentrations at the initial time, certain time t, and equilibrium point in terms of phosphorous (mg P L^{-1}). V is the volume of solution (L) and m is the mass of the material (g).

In the simultaneous adsorption of phosphate, Mg, and Ca, 0.25 g of resin was added into 50 mL of a solution containing 20 mg P L^{-1} for phosphate, 224 mg L^{-1} of calcium, and 185 mg L^{-1} of magnesium. Other conditions were kept the same as in the previous phosphate adsorption experiment. After that, the solution was taken for analyzing phosphate by UV-Vis while calcium, magnesium, and iron were analyzed by atomic absorption spectroscopy (AAS, AAnalyst 400, PerkinElmer, USA). The concentration of phosphate in the experimental process was determined according to "Standard Methods for the Examination of Water and Wastewater - 4500-P E. Ascorbic Acid Method (SMEWW 4500-P-E 2012)" and the concentrations of calcium and magnesium in the solution were determined by "Standard Methods for the Examination of Water and Wastewater - 3111 B. Direct Air-Acetylene Flame Method - Metals By Flame Atomic Absorption Spectrometry (SMEWW 3111 B 2017)".

DATA AVAILABILITY

All data generated or analyzed during this study are included in this published article and its supplementary information files. The other datasets generated during and/or analyzed during the current study are available from the corresponding author on reasonable request.

Received: 3 January 2022; Accepted: 22 August 2022;
Published online: 12 September 2022

REFERENCES

1. Sun, L., Tong, H., Gao, C., Liu, Y. & Feng, C. Removal of antibiotic resistance genes from secondary effluent by processes combining nano-iron, ultrasound-activated persulfate, and ultrafiltration. *Water Sci. Technol.* **83**, 1578–1590 (2021).
2. Zhao, D. & Sengupta, A. K. Ultimate removal of phosphate from wastewater using a new class of polymeric ion exchangers. *Water Res.* **32**, 1613–1625 (1998).
3. Mueller, D. K. & Helsel, D. R. *Nutrients in the Nation's Waters-Too Much of a Good Thing?* Vol. 1136 (BiblioGov, 2013).
4. Anzecc, A. Australian and New Zealand guidelines for fresh and marine water quality. *Aust. N.Z. Environ. Conserv. Counc. Agriculture Resour. Manag. Counc. Aust. N.Z., Canberra* **1**, 1–314 (2000).
5. Ayyasamy, P. M. et al. Two-stage removal of nitrate from groundwater using biological and chemical treatments. *J. Biosci. Bioeng.* **104**, 129–134 (2007).
6. Bassin, J. P., Kleerebezem, R., Dezotti, M. & van Loosdrecht, M. C. M. Simultaneous nitrogen and phosphate removal in aerobic granular sludge reactors operated at different temperatures. *Water Res.* **46**, 3805–3816 (2012).
7. Lu, N. C. & Liu, J. C. Removal of phosphate and fluoride from wastewater by a hybrid precipitation–microfiltration process. *Sep. Purif. Technol.* **74**, 329–335 (2010).
8. Nguyen, T. T., Le, T. T., Phan, P. T. & Nguyen, N. H. Preparation, characterization, and application of novel ferric oxide-amine material for removal of nitrate and phosphate in water. *J. Chem.* **2020**, 8583543 (2020).
9. Wiriyathamcharoen, S. et al. Synthesis optimization of hybrid anion exchanger containing triethylamine functional groups and hydrated Fe(III) oxide nanoparticles for simultaneous nitrate and phosphate removal. *Chem. Eng. J.* **381**, 122671 (2020).
10. Razali, M., Zhao, Y. Q. & Bruen, M. Effectiveness of a drinking-water treatment sludge in removing different phosphorus species from aqueous solution. *Sep. Purif. Technol.* **55**, 300–306 (2007).
11. You, X. et al. Phosphate removal from aqueous solutions using a hybrid fibrous exchanger containing hydrated ferric oxide nanoparticles. *J. Environ. Chem. Eng.* **4**, 388–397 (2016).
12. Awual, M. R. et al. Enhanced trace phosphate removal from water by zirconium(IV) loaded fibrous adsorbent. *Water Res.* **45**, 4592–4600 (2011).
13. Zhang, B., Chen, N., Feng, C. & Zhang, Z. Adsorption for phosphate by cross-linked/non-crosslinked-chitosan-Fe(III) complex sorbents: Characteristic and mechanism. *Chem. Eng. J.* **353**, 361–372 (2018).
14. Acelas, N. Y., Martin, B. D., López, D. & Jefferson, B. Selective removal of phosphate from wastewater using hydrated metal oxides dispersed within anionic exchange media. *Chemosphere* **119**, 1353–1360 (2015).
15. Zeng, L., Li, X. & Liu, J. Adsorptive removal of phosphate from aqueous solutions using iron oxide tailings. *Water Res.* **38**, 1318–1326 (2004).
16. Rubenowitz, E., Axelsson, G. & Rylander, R. Magnesium in drinking water and death from acute myocardial infarction. *Am. J. Epidemiol.* **143**, 456–462 (1996).
17. Rapant, S., Cvečková, V., Fajčíková, K., Sedláková, D. & Stehlíková, B. Impact of calcium and magnesium in groundwater and drinking water on the health of inhabitants of the Slovak Republic. *Int. J. Environ. Res. Public Health* **14**, 278 (2017).
18. Entezari, M. H. & Tahmasbi, M. Water softening by combination of ultrasound and ion exchange. *Ultrason. Sonochem.* **16**, 356–360 (2009).
19. Cinar, S. & Beler-Baykal, B. Ion exchange with natural zeolites: an alternative for water softening? *Water Sci. Technol.* **51**, 71–77 (2005).
20. Schaep, J. et al. Removal of hardness from groundwater by nanofiltration. *Desalination* **119**, 295–301 (1998).
21. Rajan, C. S. Nanotechnology in groundwater remediation. *Int. J. Environ. Sci. Develop.* **2**, https://doi.org/10.7763/IJESD.2011.V2.121 (2011).
22. Liu, W., Singh, R. P., Jothivel, S. & Fu, D. Evaluation of groundwater hardness removal using activated clinoptilolite. *Environ. Sci. Pollut. Res.* **27**, 17541–17549 (2020).
23. Baliarsingh, N., Parida, K. & Pradhan, G. Influence of the nature and concentration of precursor metal ions in the brucite layer of LDHs for phosphate adsorption—a review. *RSC Adv.* **3**, 23865 (2013).
24. Chubar, N. I. et al. Adsorption of phosphate ions on novel inorganic ion exchangers. *Colloids Surf. A: Physicochemical Eng. Asp.* **255**, 55–63 (2005).
25. Jellali, S., Wahab, M. A., Hassine, R. B., Hamzaoui, A. H. & Bousselmi, L. Adsorption characteristics of phosphorus from aqueous solutions onto phosphate mine wastes. *Chem. Eng. J.* **169**, 157–165 (2011).
26. Huang, W. et al. Phosphate removal from wastewater using red mud. *J. Hazard. Mater.* **158**, 35–42 (2008).
27. Awual, M. R., Urata, S., Jyo, A., Tamada, M. & Katakai, A. Arsenate removal from water by a weak-base anion exchange fibrous adsorbent. *Water Res.* **42**, 689–696 (2008).
28. Awual, M. R. & Jyo, A. Assessing of phosphorus removal by polymeric anion exchangers. *Desalination* **281**, 111–117 (2011).
29. Chen, J. et al. Phosphate immobilization from aqueous solution by fly ashes in relation to their composition. *J. Hazard. Mater.* **139**, 293–300 (2007).
30. Reddy, D. H. K. & Lee, S.-M. Application of magnetic chitosan composites for the removal of toxic metal and dyes from aqueous solutions. *Adv. Colloid Interface Sci.* **201–202**, 68–93 (2013).
31. Biswas, B. K. et al. Removal and recovery of phosphorus from water by means of adsorption onto orange waste gel loaded with zirconium. *Bioresour. Technol.* **99**, 8685–8690 (2008).
32. Sherman, D. M. & Randall, S. R. Surface complexation of arsenic(V) to iron(III) (hydr)oxides: structural mechanism from ab initio molecular geometries and EXAFS spectroscopy. *Geochimica et. Cosmochimica Acta* **67**, 4223–4230 (2003).
33. Blaney, L. M., Cinar, S. & SenGupta, A. K. Hybrid anion exchanger for trace phosphate removal from water and wastewater. *Water Res.* **41**, 1603–1613 (2007).
34. Sengupta, S. & Pandit, A. Selective removal of phosphorus from wastewater combined with its recovery as a solid-phase fertilizer. *Water Res.* **45**, 3318–3330 (2011).
35. Zhu, X. & Jyo, A. Column-mode phosphate removal by a novel highly selective adsorbent. *Water Res.* **39**, 2301–2308 (2005).
36. Awual, M. R., Jyo, A., El-Safty, S. A., Tamada, M. & Seko, N. A weak-base fibrous anion exchanger effective for rapid phosphate removal from water. *J. Hazard. Mater.* **188**, 164–171 (2011).
37. DeMarco, M. J., SenGupta, A. K. & Greenleaf, J. E. Arsenic removal using a polymeric/inorganic hybrid sorbent. *Water Res.* **37**, 164–176 (2003).
38. Mahmudov, R. & Huang, C. P. Selective adsorption of oxyanions on activated carbon exemplified by Filtrasorb 400 (F400). *Sep. Purif. Technol.* **77**, 294–300 (2011).
39. Cumbal, L. & SenGupta, A. K. Arsenic removal using polymer-supported hydrated iron(III) oxide nanoparticles: role of Donnan membrane effect. *Environ. Sci. Technol.* **39**, 6508–6515 (2005).
40. Nguyen, T. T. et al. Synthesis of cation exchange resin-supported iron and magnesium oxides/hydroxides composite for nitrate removal in water. *Chin. J. Chem. Eng.* **32**, 378–384 (2021).

41. Nguyen, T. T. et al. Synthesis of natural flowerlike iron-alum oxide with special interaction of Fe-Si-Al oxides as an effective catalyst for heterogeneous Fenton process. *J. Environ. Chem. Eng.* **9**, 105732 (2021).
42. Claff, S. R., Sullivan, L. A., Burton, E. D. & Bush, R. T. A sequential extraction procedure for acid sulfate soils: partitioning of iron. *Geoderma* **155**, 224–230 (2010).
43. Sowmya, A. & Meenakshi, S. Removal of nitrate and phosphate anions from aqueous solutions using strong base anion exchange resin. *Desalin. Water Treat.* **51**, 7145–7156 (2013).
44. Lazar, L. et al. FTIR analysis of ion exchange resins with application in permanent hard water softening. *Environ. Eng. Manag. J.* **13**, 2145–2152 (2014).
45. Lee, B. et al. Synthesis and characterization of organic−inorganic hybrid mesoporous anion-exchange resins for perrhenate (ReO4-) anion adsorption. *Langmuir* **19**, 4246–4252 (2003).
46. Liao, S. et al. Structure and Mn^{2+} adsorption properties of boron-doped goethite. *Appl. Clay Sci.* **38**, 43–50 (2007).
47. Ruan, H. D., Frost, R. L., Kloprogge, J. T. & Duong, L. Infrared spectroscopy of goethite dehydroxylation. II. Effect of aluminium substitution on the behaviour of hydroxyl units. *Spectrochimica Acta Part A: Mol. Biomolecular Spectrosc.* **58**, 479–491 (2002).
48. Rahimi, S., Moattari, R. M., Rajabi, L., Derakhshan, A. A. & Keyhani, M. Iron oxide/hydroxide (α,γ-FeOOH) nanoparticles as high potential adsorbents for lead removal from polluted aquatic media. *J. Ind. Eng. Chem.* **23**, 33–43 (2015).
49. Zhang, Y. et al. Preparation of β-$Ca_3(PO_4)_2$ bioceramic powder from calcium carbonate and phosphoric acid. *Curr. Appl. Phys.* **5**, 531–534 (2005).
50. Ghosh, S., Dhole, K., Tripathy, M. K., Kumar, R. & Sharma, R. S. FTIR spectroscopy in the characterization of the mixture of nuclear grade cation and anion exchange resins. *J. Radioanalytical Nucl. Chem.* **304**, 917–923 (2015).
51. Harbi, S., Guesmi, F., Tabassi, D., Hannachi, C. & Hamrouni, B. Application of response surface methodology and artificial neural network: Modeling and optimization of Cr(VI) adsorption process using Dowex 1×8 anion exchange resin. *Water Sci. Technol.* **73**, https://doi.org/10.2166/wst.2016.091 (2016).
52. Raul, P., Devi, R., Umlong, I., Banerjee, S. & Purkait, M. Removal of fluoride from water using iron oxide-hydroxide nanoparticles. *J. Nanosci. Nanotechnol.* **12**, 3922–3930 (2012).
53. Nur, T., Johir, M. A. H., Loganathan, P., Nguyen, T. V. & Kandasamy, J. Phosphate removal from water using an iron oxide impregnated strong base anion exchange resin. *J. Ind. Eng. Chem.* **20**, 1301–1307 (2014).
54. Khoualdia, B., Loungou, M. & Elaloui, E. Adsorption of organic matter from industrial phosphoric acid (H_3PO_4) onto activated bentonite. *Arab. J. Chem.* **10**, S1073–S1080 (2017).
55. Limousin, G. et al. Sorption isotherms: a review on physical bases, modeling and measurement. *Appl. Geochem.* **22**, 249–275 (2007).
56. Venkiteshwaran, K., Wells, E. & Mayer, B. K. Kinetics, affinity, thermodynamics, and selectivity of phosphate removal using immobilized phosphate-binding proteins. *Environ. Sci. Technol.* **54**, 10885–10894 (2020).
57. Ren, J., Li, N., Zhao, L. & Ren, N. Enhanced adsorption of phosphate by loading nanosized ferric oxyhydroxide on anion resin. *Front. Environ. Sci. Eng.* **8**, 531–538 (2014).
58. Belhachemi, M. & Addoun, F. Comparative adsorption isotherms and modeling of methylene blue onto activated carbons. *Appl. Water Sci.* **1**, 111–117 (2011).
59. Chabani, M., Amrane, A. & Bensmaili, A. Equilibrium sorption isotherms for nitrate on resin Amberlite IRA 400. *J. Hazard. Mater.* **165**, 27–33 (2009).
60. Das, R., Das Tuhi, S. & Zaidi, S. M. J. In *Carbon Nanotubes for Clean Water* (ed. Rasel Das) 85–106 (Springer International Publishing, 2018).
61. Bekçi, Z., Seki, Y. & Kadir Yurdakoç, M. A study of equilibrium and FTIR, SEM/EDS analysis of trimethoprim adsorption onto K10. *J. Mol. Struct.* **827**, 67–74 (2007).
62. Du, X. et al. Insights into protein–ligand interactions: mechanisms, models, and methods. *Int. J. Mol. Sci.* **17**, 144 (2016).

ACKNOWLEDGEMENTS

This research is funded by Vietnam National University - Ho Chi Minh City under grant number A2020-16-01.

AUTHOR CONTRIBUTIONS

L.B.T. carried out the experiments and data processing and drafted the manuscript. T.T.N. conceived of the idea, designed the experiments, and supervised the study. S.P., Q.A.N.T., and T.T.L. carried out some experiments and data processing. N.H.N. drafted and revised the manuscript.

COMPETING INTERESTS

The authors declare no competing interests.

ADDITIONAL INFORMATION

Supplementary information The online version contains supplementary material available at https://doi.org/10.1038/s41545-022-00188-9.

Correspondence and requests for materials should be addressed to Trung Thanh Nguyen or Nhat Huy Nguyen.

Reprints and permission information is available at http://www.nature.com/reprints

Publisher's note Springer Nature remains neutral with regard to jurisdictional claims in published maps and institutional affiliations.